Electronic Supplementary information for the article

Bright luminescence of new low-melting copper(I) chlorides with compact organic cations

Daria E. Belikova[a], Sergey A. Fateev[a], Victor N. Khrustalev[bc], Vladislava Y. Kozhevnikova[d], Artem A. Ordinartsev[a], Alexander V. Dzuban[d], Eugene A. Goodilin[ad], Alexey B. Tarasov[ad†]

a. Laboratory of New Materials for Solar Energetics, Faculty of Materials Science, Lomonosov Moscow State University, 119991 Moscow, Russian Federation.

b. Inorganic Chemistry Department, Peoples' Friendship University of Russia (RUDN University), 117198 Moscow, Russian Federation.

c. Zelinsky Institute of Organic Chemistry, Russian Academy of Sciences, Leninsky Prosp. 47, Moscow 119991, Russia.

d. Department of Chemistry, Lomonosov Moscow State University, 119991 Moscow, Russian Federation

† These authors have contributed equally.

* Corresponding author: alexey.bor.tarasov@yandex.ru

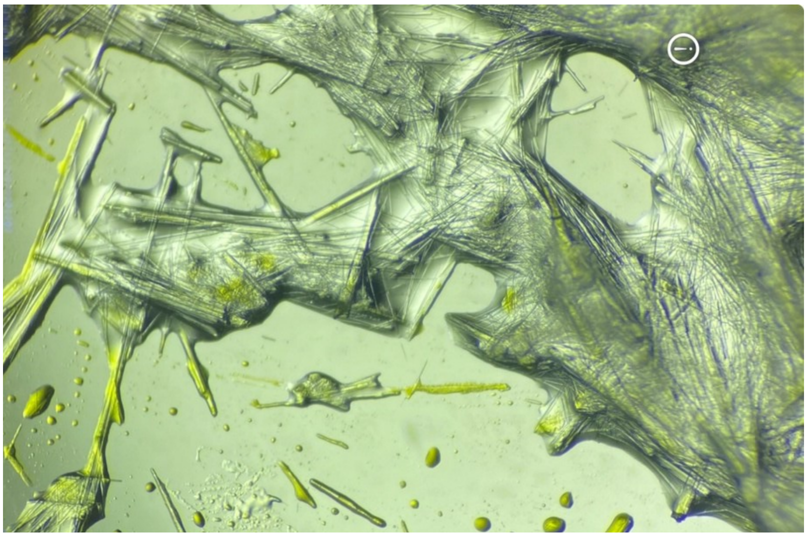

Figure S1. Photo of synthesized $AcCuCl_2$ needle-like crystals in optical microscope.

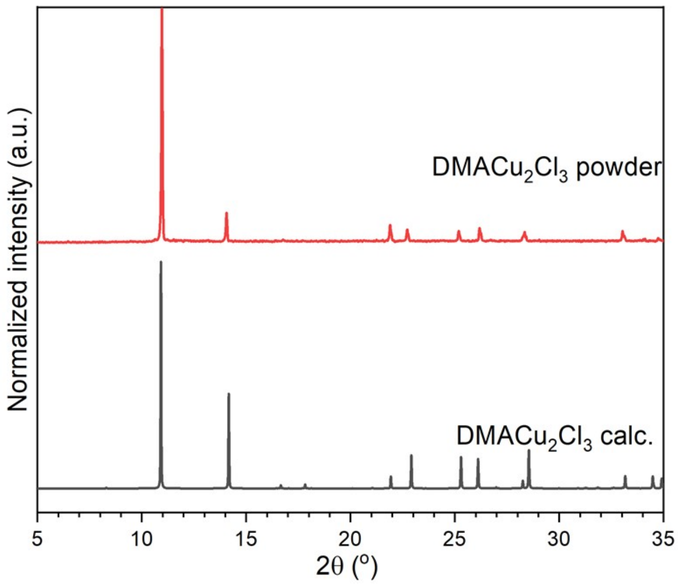

Figure S2. XRD pattern of the synthesized $DMACu_2Cl_3$ powder in comparison with the calculated pattern.

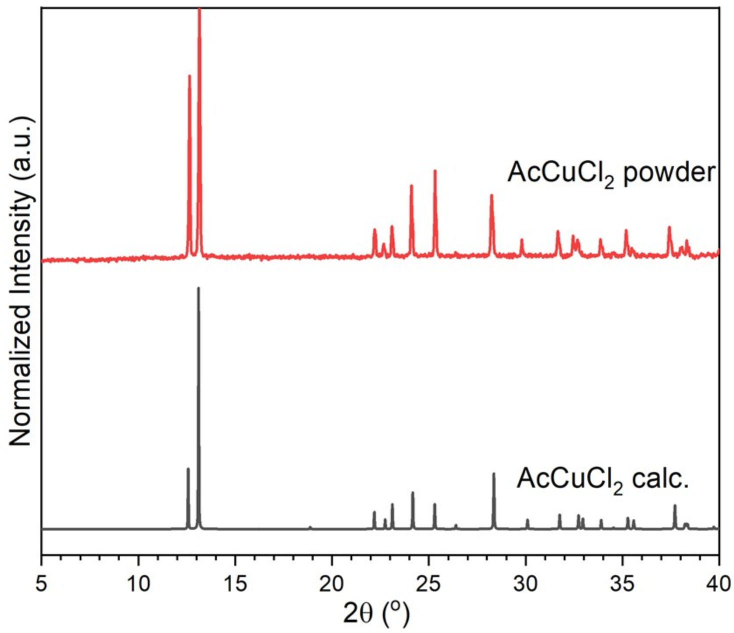

Figure S3. XRD pattern of the synthesized $AcCuCl_2$ powder in comparison with the calculated pattern.

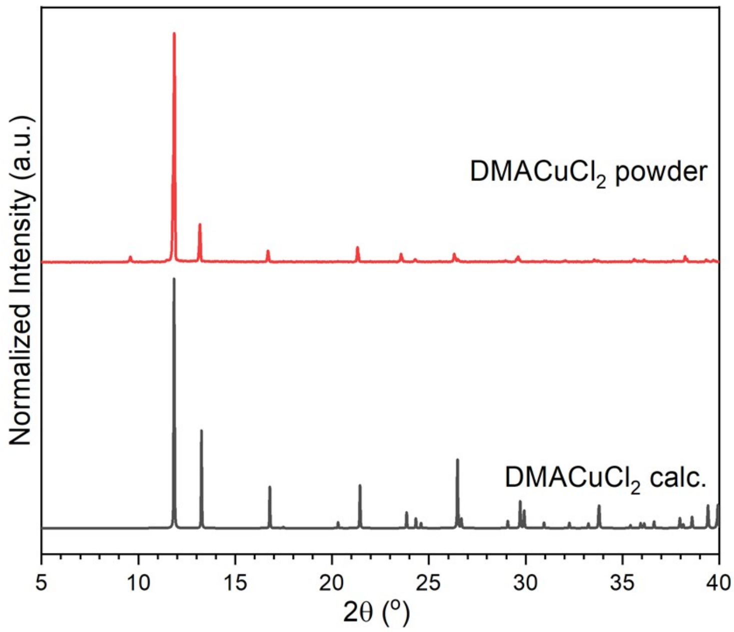

Figure S4. XRD pattern of the synthesized $DMACuCl_2$ powder in comparison with the calculated pattern.

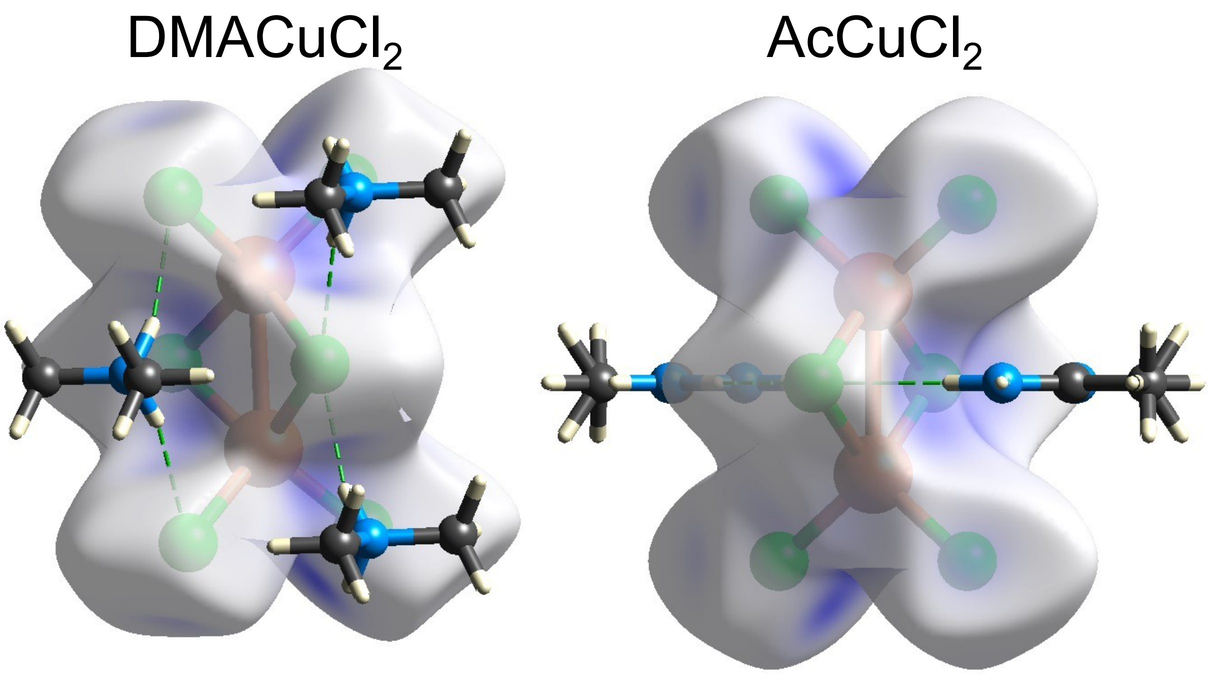

Figure S5. Hirschfeld surfaces of the elementary units of the inorganic framework for $DMACuCl_2$ and $AcCuCl_2$ phases.

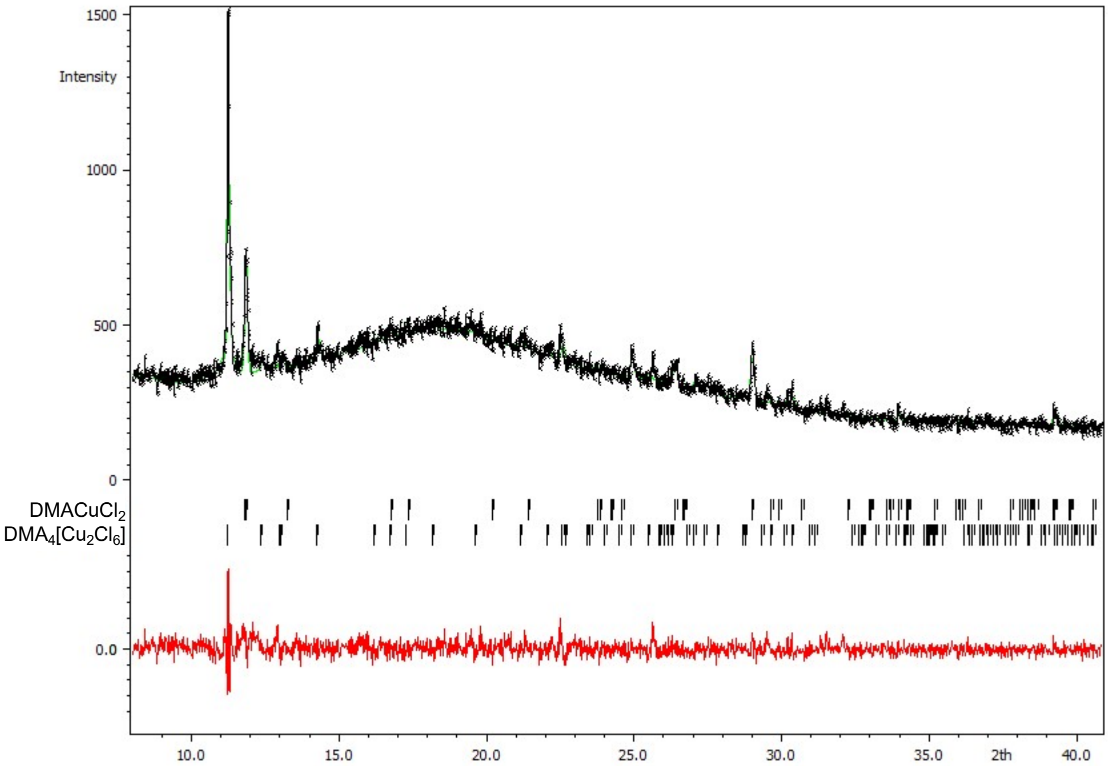

Figure S6. Refined XRD pattern of $DMA_4[Cu_2Cl_6]$. The black and green curves represent the experimental data and the calculated profile, respectively. The difference curve is plotted in red at the bottom of the pattern. Phase #1 and Phase #2 correspond to $DMA_4[Cu_2Cl_6]$ and $DMACuCl_2$ phases, respectively.

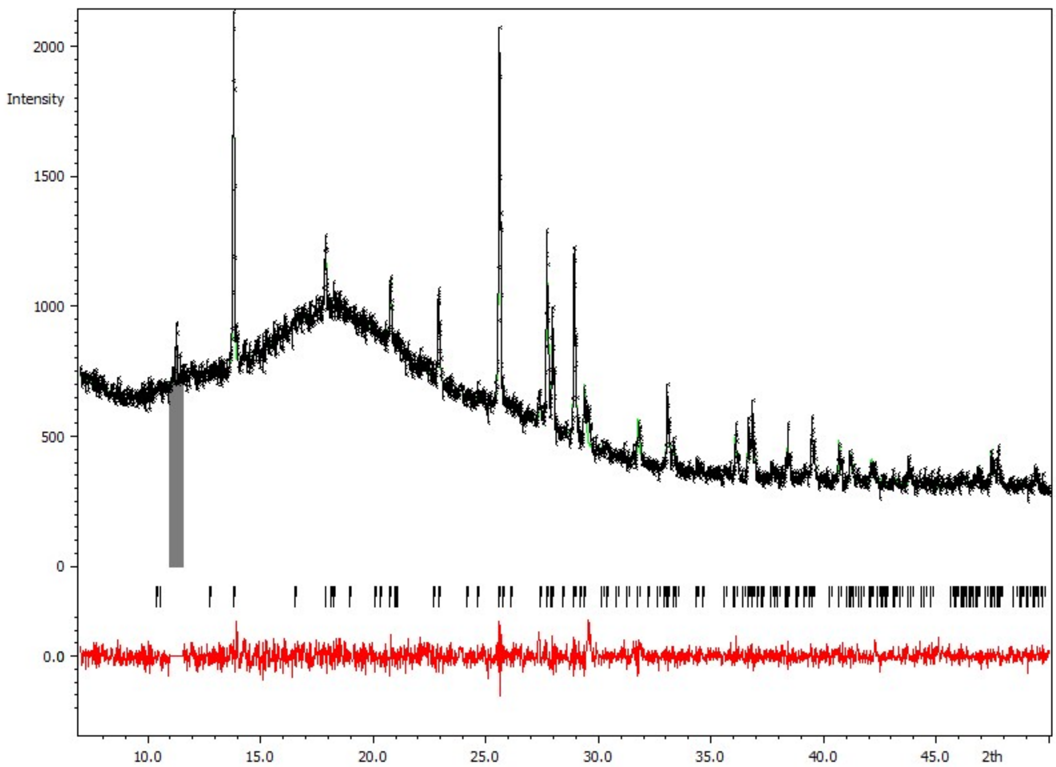

Figure S7. Refined XRD pattern of DMA_3CuCl_4. The black and green curves represent the experimental data and the calculated profile, respectively. The difference curve is plotted in red at the bottom of the pattern. The excluded reflex corresponds to the $DMA_4[Cu_2Cl_6]$ phase.

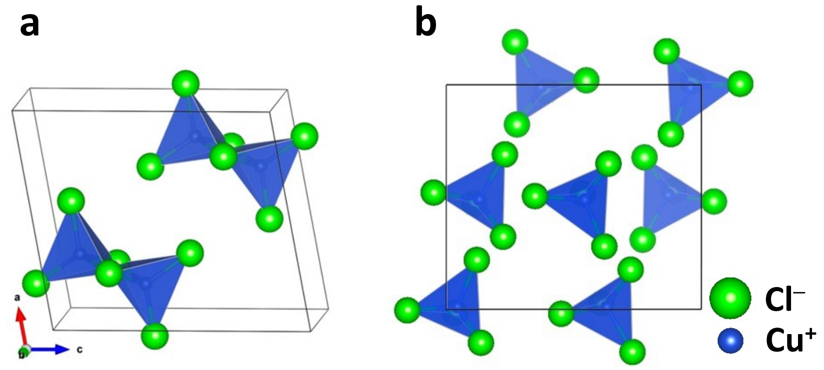

Figure S8. Models of anionic frameworks for a) $DMA_4[Cu_2Cl_6]$ and b) DMA_3CuCl_4 phases.

Table S1. Bond length distortion index and bond angle dispersion values for the studied phases.

Phase	Cu-Cl bond length, Å	Distortion index (bond length)	Cl-Cu-Cl angles, deg.	Bond angle variance, deg.^{2}	Shortest Cl···H distance**, Å
$DMACu_2Cl_3$	2.2852(5) 2.2781(5) 2.5389(5) 2.4436(5)	0.044	128.26(3) 109.964(17) 105.217(17) 105.145(19) 103.572(17) 102.425(17)	94.88	2.57(3)
$DMACuCl_2$	2.2583(5) 2.5540(6) 2.2583(5) 2.5540(6)	0.062	137.54(4) 107.500(19) 107.500(19) 101.361(15) 101.361(15) 93.19(3)	238.43	2.2961(3)
$AcCuCl_2$	2.3598(7) 2.3762(6) 2.3762(6) 2.3598(7)	0.00347	113.100(8) 113.100(8) 113.100(8) 113.100(8) 104.16(3) 100.65(3)	31.74	2.54(3)

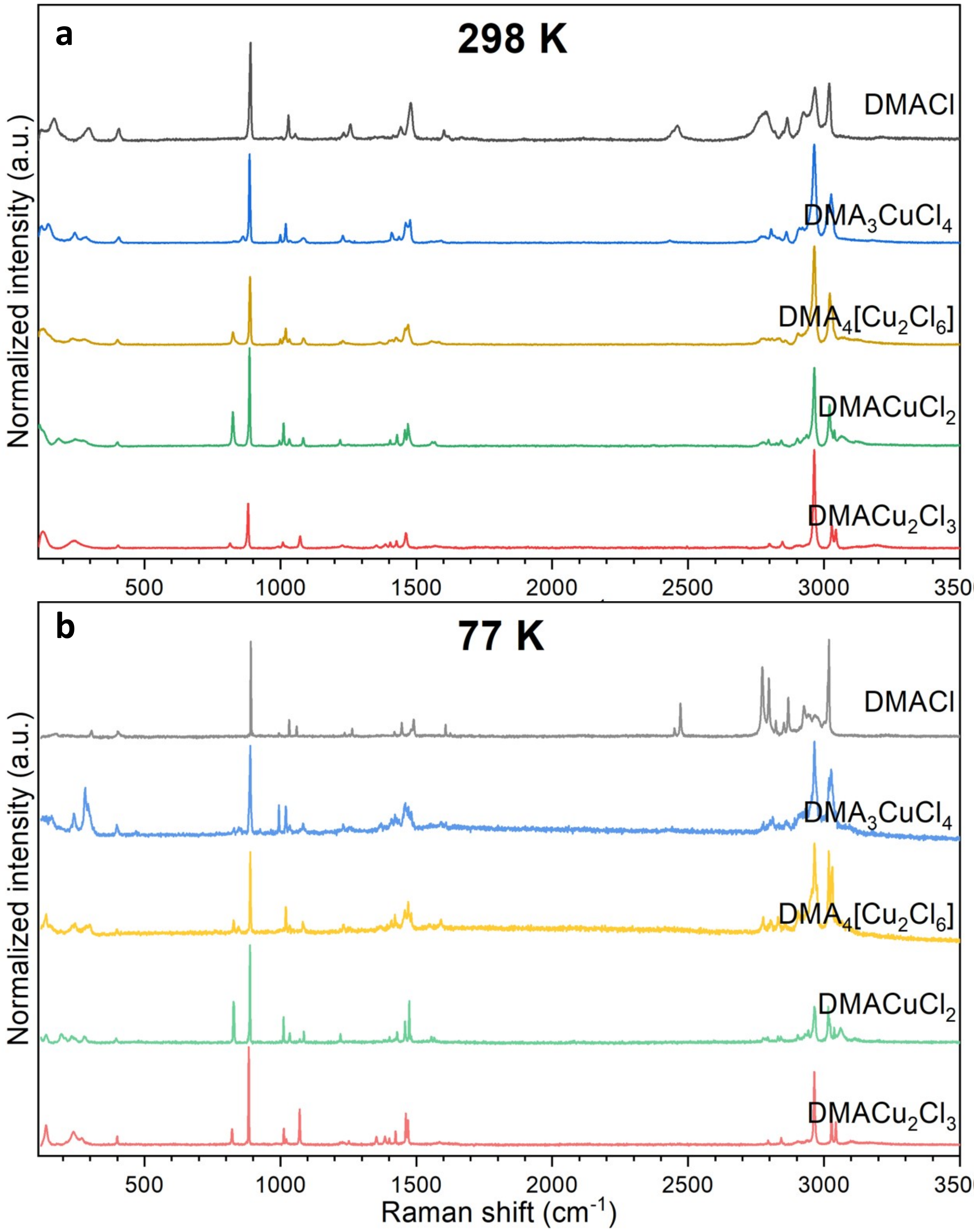

Figure S9. Raman spectra of studied hybrid copper(I) halides with DMA^+ cation recorded at a) room temperature and b) 77 K.

Analysis of the Raman spectra

Based on existing data on Raman modes of other hybrid halometallates with dimethylammonium cations [1–3], we interpreted the strong modes in the fingerprint region of the spectra as NC_2 scissoring at 401 – 406 cm^{-1} (NC_2 δ_{sc}), NH_2^+ rocking at 814 – 862 cm^{-1} (NH_2^+ δ_r), symmetrical and asymmetrical NC_2 stretching at 881 – 890 cm^{-1} (NC_2 ν_s) and 993 – 1084 cm^{-1} (N-C ν_{as}), respectively. Other present modes correspond to NC_2 wagging and twisting at 1219 – 1257 cm^{-1} (NC_2 δ_w, δ_t), NH_2^+ wagging at 1350 – 1425 cm^{-1} (NH_2^+ δ_w) and CH_3 angle-bending deformation at 1450 – 1500 cm^{-1} (CH_3 δ_b). In the 2700 – 3200 cm^{-1} region we observe four typical areas corresponding to symmetrical (ν_s) and asymmetrical (ν_{as}) CH_3 and NH_2^+ stretching. Full list of interpreted peaks is presented in Table S2.

Table S2. Models of anionic frameworks for a) $DMA_4[Cu_2Cl_6]$ and b) DMA_3CuCl_4 phases.

Vibrational frequency, cm^{-1}										Assignment
DMACl		DMA_3CuCl_4		DMA_2CuCl_3		$DMACuCl_2$		$DMACu_2Cl_3$		
298 K	77 K	298 K	77 K	298 K	77 K	298 K	77 K	298 K	77 K	
169 w 295 w	173 w 305 w	146 m 243 w 283 w	158 w 240 w 282 m	129 w 236 w 279 w	242 w 289 w	131 w 184 w 254 w	137 w 194 w 231 w 280 w	128 w 239 w	137 m 238 w 267 w	lattice modes
406 w	401 w	405 w	398 w	400 w	397 w	401 vw	395 w	403 vw	400 w	NC_2 scissoring δ_{sc}
		863 w	828 vw 847 vw	825 w	827 w 846 vw	825 m	828 m	815 w	822 w	NH_2^+ rocking δ_r
890 s	891 s	886 s	889 s	888 s	889 s	886 s	888 s	881 m	883 s	symmetrical NC_2 stretching ν_s
1002 vw 1029 w 1054 w	1011 w 1020 vw 1032 w	999 w 1019 w 1035 vw	994 m 1020 m 1036 w	999 vw 1012 w 1019 vw 1033 vw	1000 vw 1012 vw 1020 m 1035 w	996 vw 1012 m 1032 w	1011 m 1035 w	1008 vw	1012 w 1021 vw	asymmetrical NC_2 stretching ν_{as}
	1060 w	1084 w	1085 w	1085 w	1083 w	1084 w	1072 vw 1086 w	1073 w	1071 m	
1232 w	1236 vw	1229 w	1229 w	1231 vw	1232 w	1219 w	1220 w	1228 vw	1229 vw	NC_2 wagging δ_w
1258 w	1246 vw	1253 vw	1256 vw	1250 vw	1252 vw	1249 w		1246 vw	1252 vw	NC_2 twisting δ_t
1442 w	1419 vw 1446 w	1371 vw 1409 w 1436 vw	1367 w 1380 vw 1393 vw 1408 w 1421 vw 1427 vw 1437 vw	1402 vw 1413 vw 1424 vw 1427 vw	1369 vw 1393 vw 1406 w 1420 w	1403 w 1429 w	1400 vw 1430 w	1353 vw 1388 vw 1403 vw 1429 vw	1352 w 1384 w 1400 vw 1423 w	NH_2^+ wagging δ_w
1479 m	1481 vw 1490 w	1460 w 1477 w	1457 m 1465 w 1471 w 1476 w 1482 w 1491 w	1458 w 1470 w	1457 w 1470 m 1481 w	1459 w 1470 w	1459 w 1473 m 1481 vw	1460 w	1461 m 1469 m	CH_3 angle-bending deformation δ_b
1602 w 1619 w	1607 w 1625 vw	1554 vw 1591 vw	1546 w	1554 vw 1584 vw	1549 vw	1559 vw 1569 vw	1555 vw 1565 vw	1567 vw	1785 vw	NH_2^+ scissoring δ_s
2461 m	2449 w 2471 m									?
2786 m 2865 m	2772 s 2797 s	2805 w 2861 w	2802 vw 2810 vw	2802 w 2861 w	2775 w 2803 w	2794 w 2843 w	2780 vw 2793 vw	2800 w 2861 w	2794 vw 2842 vw	symmetrical CH_3

	2823 w 2831 vw 2852 w 2868 m		2862 vw		2832 w 2857 w		2831 vw 2842 vw			stretching ν_s, overtones of CH_3 δ_b
2923 m	2910 vw 2925 m	2905 w	2892 vw 2911 w	2904 w	2909 w 2934 w	2901 w	2904 vw 2929 vw 2940 w	2905 vw	2902 vw	symmetrical NH_2^+ stretching ν_s
2966 m	2945 w 2968 w	2963 s	2963 s 2984 vw	2963 s	2955 m 2966 s 2973 m	2964 s	2965 s	2964 s	2937 vw 2964 s	asymmetrical CH_3 stretching ν_{as}
3019 m	3001 w 3019 s	3014 m 3026 m	3018 m 3026 m	3020 m 3030 m	3017 s 3029 s	3020 m 3038 w	3015 s 3020 m 3039 w	3028 m 3043 w	3028 m 3043 w	asymmetrical NH_2^+ stretching ν_{as}

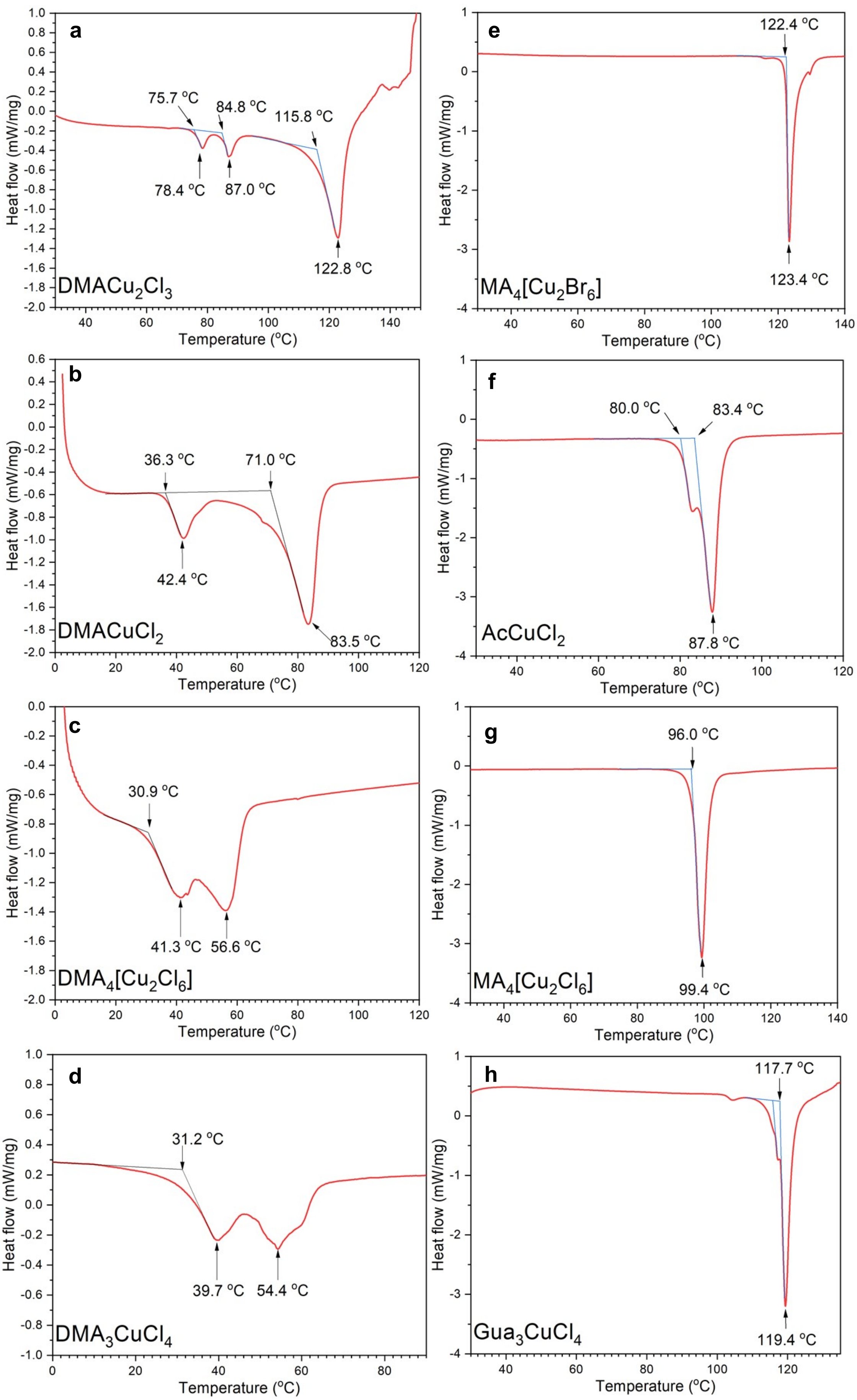

Figure S10. Differential scanning calorimetry heating curves for the studied phases of hybrid copper(I) halides.

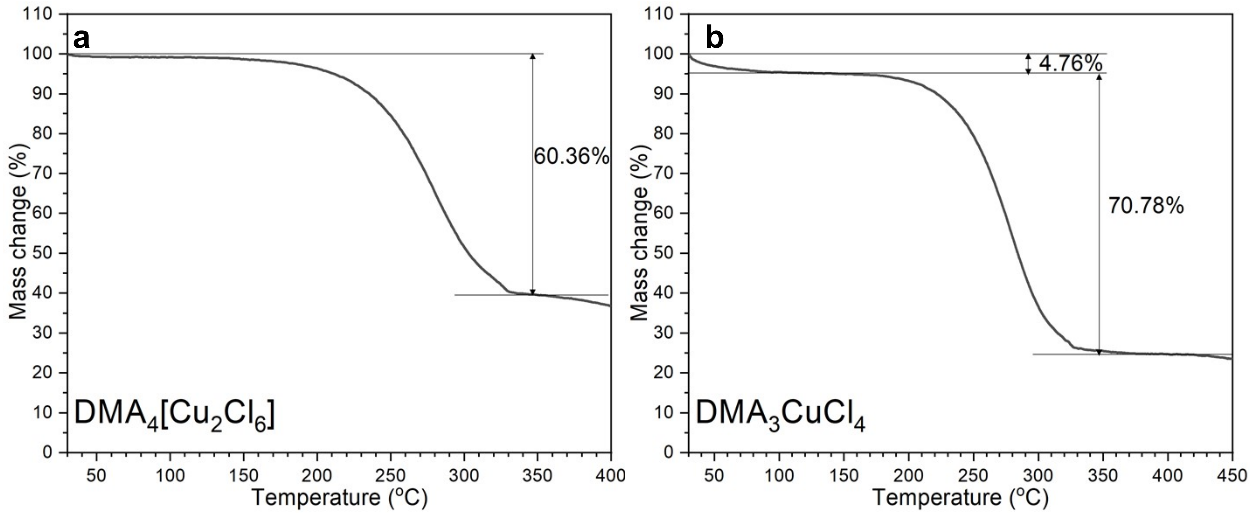

Figure S11. Thermogravimetric curves for melt-processed a) DMA4[Cu_2Cl_6] (theoretical mass change is 62.22%) and b) DMA_3CuCl_4 (theoretical mass change is 71.18%).

References

1 J. T. Edsall, *J. Chem. Phys.*, 2004, **5**, 225–237.

2 G. Bator, R. Jakubas, J. Lefebvre and Y. Guinet, *Vib. Spectrosc.*, 1998, **18**, 203–210.

3 M. Wojtaś, G. Bator and J. Baran, *Vib. Spectrosc.*, 2003, **33**, 143–152.